

## Charge density waves in monolayer and few-layer NbS<sub>2</sub> and phase modulation by doping, thickness, and temperature

Peng Wu, Xiangyang Peng <sup>\*</sup>, Chaobo Luo , Zhenqing Li , and Jianxin Zhong <sup>†</sup>

Hunan Key Laboratory for Micro-Nano Energy Materials and Devices, School of Physics and Optoelectronics, Xiangtan University, Hunan 411105, People's Republic of China



(Received 12 March 2021; revised 14 April 2022; accepted 18 April 2022; published 9 May 2022)

By carrying out first-principles calculations, we studied the charge density waves (CDWs) in monolayer/few-layer  $H$ -NbS<sub>2</sub>. For monolayer NbS<sub>2</sub>, unstable phonon modes are found to develop at the  $2/3\Gamma$ M point and its symmetric points in the whole Brillouin zone. By displacing the atoms along the unstable mode, a new dynamically stable  $3 \times 3$  structure with lower total energy is obtained, which corresponds well to the experimentally observed  $3 \times 3$  CDW phase. The symmetries are broken in the  $3 \times 3$  CDW phase, leading to gap opening and anisotropic properties. The  $3 \times 3$  CDW phase of NbS<sub>2</sub> is found to be stable with respect to small strains. In comparison with NbSe<sub>2</sub>, it is found that the Se atoms are much more active in vibration than the S atoms, resulting in the different CDW behaviors in these two very similar materials. We explored the CDW phase tuning by electron doping, and a sequence of CDW phase transitions from  $3 \times 3$  to  $2 \times 2$  and to  $4\sqrt{3} \times 4\sqrt{3}$  is found. The doping-dependent CDW phase provides insight into the inconsistent observation of CDW phases in NbS<sub>2</sub>/graphene and NbS<sub>2</sub>/Au(111) based on the difference in substrate charge doping. We further investigated the CDW phases of the bilayer and trilayer NbS<sub>2</sub>. With the decrease of the temperature, a series of instabilities occur in the phonon spectrum of bilayer NbS<sub>2</sub>, which correspond to  $2 \times 2$ ,  $3 \times 3$ , and  $4 \times 4$  CDW phases. For trilayer NbS<sub>2</sub>, in contrast, only a  $2 \times 2$  CDW phase is found, whereas the  $3 \times 3$  CDW phase, which exists in monolayer and bilayer, is not manifested even at ultralow temperature. The layer-dependent CDW phases indicate significant effects of interlayer interactions.

DOI: [10.1103/PhysRevB.105.174105](https://doi.org/10.1103/PhysRevB.105.174105)

### I. INTRODUCTION

Recently, transition-metal dichalcogenides (TMDs) have become a focus of condensed matter physics due to their excellent properties [1–7], rendering them highly fascinating for fundamental studies of novel physics and technological exploration of advanced applications. TMDs are  $MX_2$ -type materials formed by van der Waals (vdW) layers containing a transition metal  $M$  sublayer (e.g., Mo, W, V, Nb, and Ta) sandwiched between two sulfur  $X$  sublayers (e.g., S, Se, and Te). Two-dimensional (2D) TMDs exhibit versatile and superb properties. Group VI TMD monolayers of hexagonal structure, such as MoS<sub>2</sub> and WSe<sub>2</sub> [8–10], are ideal photoelectronic materials with direct band gaps from near-infrared to the visible region. They also possess a new degree of quantum freedom—a valley—to present Berry phase-related physics such as the valley-spin Hall effect [11]. When they are in  $1T'$  form, they become quantum spin Hall insulators.

On the other hand, group V TMDs, e.g., NbSe<sub>2</sub>, TaSe<sub>2</sub>, and TaS<sub>2</sub>, are distinguished by a different theme, namely charge density waves (CDW) [12–14] and the related superconductivity [1,15–22]. One dimensional CDW driven by Peierls instability was predicted and observed, leading to a distortion of the lattice and energy gap opening at the Fermi level [23,24]. The recent discovery of CDWs in quasi-2D systems,

such as  $2H$  and  $1T$ -TaS<sub>2</sub> and TaSe<sub>2</sub>, and in  $2H$ -NbSe<sub>2</sub>, has sparked keen and renewed interest in CDW phases. Experimental and computational studies found that when the bulk  $2H$ -NbSe<sub>2</sub> is reduced to a monolayer  $H$ -NbSe<sub>2</sub>, the CDW phase transition temperature  $T_{CDW}$  is considerably enhanced [25,26] and simultaneously NbSe<sub>2</sub> turns from metallic to semimetallic, indicating that interlayer interaction and dimensionality have great effects on CDWs [3].

NbS<sub>2</sub> is an exception among the group V TMDs in that it only shows the superconducting phase under low temperatures, whereas the CDW phase seems to be absent, as opposed to other group V TMDs in which these two phases can coexist [27,28]. It is believed that NbS<sub>2</sub> is on the verge of a CDW phase transition, but it is suppressed by anharmonicity [7,29]. Recent experiments appear to be inconsistent. It was predicted by an anharmonic model that there is no CDW phase transition for bulk  $2H$ -NbS<sub>2</sub> [30], whereas a recent scanning tunneling microscopy experiment discovered an impurity-pinned incommensurate CDW [31]. No CDW phase was found in monolayer NbS<sub>2</sub> grown on Au(111) [32]. However, a  $3 \times 3$  CDW order was observed in the graphene-supported monolayer NbS<sub>2</sub> at ultralow temperature (4.6 K) [33]. In monolayer NbS<sub>2</sub>, the calculated phonon dispersion has imaginary frequencies occurring around  $0.72 \Gamma$ M, which is fairly close to  $2/3 \Gamma$ M and should give rise to the observed  $3 \times 3$  CDW phase [30].

The different NbS<sub>2</sub> CDW phases exhibited in bulk and 2D limits indicate that the interlayer interaction has a significant impact on the CDW phases. It is important to see how the

<sup>\*</sup>xiangyang\_peng@xtu.edu.cn

<sup>†</sup>jxzhong@xtu.edu.cn

interlayer interaction governs the CDW phase evolution on thickness. Although the low-temperature  $3 \times 3$  CDW phase of  $\text{NbS}_2$  has been observed, the distorted structure induced by the phase transition and its effects on the electronic structure are still to be understood. It is also interesting to know whether there are new CDW phases if the temperature is lowered further. The different experimental observations of the CDW phase of  $\text{NbS}_2$  on graphene and Au have suggested that substrate may play an important role in determining the presence and absence of CDW phase by charge transfer or/and strain. However, a quantitative study of charge transfer and strain is still lacking, and their effects on the CDW phases of  $\text{NbS}_2$  have yet to be confirmed. Since the CDW phase of  $\text{NbS}_2$  is sensitive to external conditions, electron doping could be a feasible means to tune the CDW phase. Motivated by the experiments, we performed first-principles calculations to determine the atomic and electronic structures of the  $3 \times 3$  CDW phase of monolayer  $\text{NbS}_2$ , and we explored the CDW phase tuning by charge doping, thickness, and temperature, which will be presented in the following.

## II. COMPUTATIONAL METHODS

The first-principles calculation is carried out by using the Vienna Ab-initio Simulation Package (VASP) [34–36] in the framework of density functional theory. The energy cutoff for plane-wave expansion is 500 eV. The local density approximation (LDA) is adopted for the exchange-correlation functional. The electron-core interaction is described by the projector augmented wave (PAW) method [37]. The Brillouin zone of the primitive unit cell is sampled by a  $\Gamma$ -centered mesh of  $30 \times 30 \times 1$  for 2D layer(s). The density of the  $k$  points is maintained as a constant, e.g., the  $k$  mesh for a  $3 \times 3$  lateral expansion of the primitive unit cell of 2D layers is a  $\Gamma$ -centered  $10 \times 10 \times 1$  mesh. In the following, the default system is the  $1 \times 1$  primitive cell of 2D  $H$ - $\text{NbS}_2$  unless otherwise stated. The partial occupancy of the bands at finite temperature is treated by the Gaussian smearing method [17,38–43]. The temperature is described by the Gaussian broadening width  $\sigma$ , which can simulate the thermal distribution of the electrons to some extent. Although the temperature estimated by  $\sigma = k_B T$  is much larger than the observed temperature due possibly to ignoring the thermal motion of ions,  $\sigma$  is often used to qualitatively account for the temperature trend [17,44]. The energy and force convergence criteria for atomic structure optimization are  $10^{-8}$  eV and  $10^{-4}$  eV/Å, respectively. The monolayer/few-layer  $\text{NbS}_2$  are modeled by slabs in periodic supercells, in which neighboring slabs are separated by a vacuum layer of 10 Å to avoid the artificial interaction between the periodic images. The calculation of the phonon dispersion is based on the density functional perturbation theory (DFPT) by using the PHONOPY package [45]. In calculations of the phonon properties, a  $15 \times 15 \times 1$   $q$ -mesh is used.

## III. RESULTS AND DISCUSSION

Monolayer  $\text{NbS}_2$  crystallizes into a hexagonal structure, containing two S sublayers sandwiching a middle Nb sublayer [Fig. 1(a)]. After cell relaxation, the optimized lattice param-

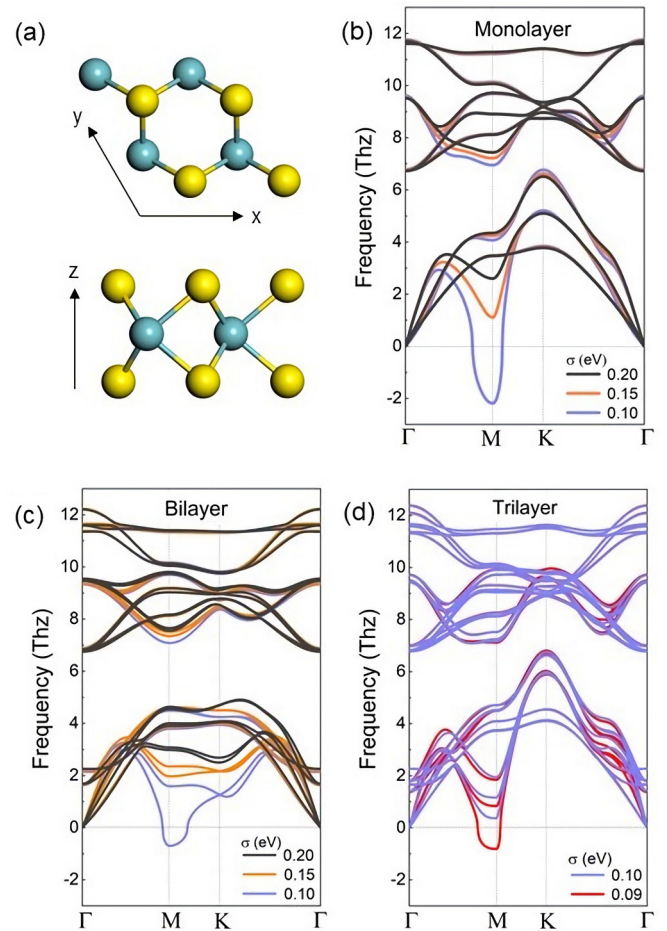


FIG. 1. The top (upper) and side (lower) views of the atomic structure of monolayer  $\text{NbS}_2$  (a) and the phonon dispersion of monolayer (b), bilayer (c), and trilayer (d)  $\text{NbS}_2$  under different temperatures ( $\sigma$ ). The green and yellow spheres in (a) denote the Nb and S atoms, respectively.

eters are obtained ( $a = b = 3.30$  Å), which are very close to the previous results [46]. In the following, the bilayer and trilayer  $\text{NbS}_2$  take the stacking order in bulk  $2H$ - $\text{NbS}_2$ . Their lateral lattice parameters are almost the same as those of the monolayer, and their interlayer distances are calculated to be 2.61 Å. We calculated the phonon spectra of monolayer/few-layer  $H$ - $\text{NbS}_2$  with respect to different  $\sigma$  to study the CDW phase transitions under different temperatures.

### A. The CDW phases at higher temperatures

The broadening parameter  $\sigma$  is scanned from 0.5 down to 0.09 eV in our calculations to study the CDW phases in the higher-temperature region. For monolayer  $\text{NbS}_2$ , there is a soft mode starting to develop at the  $M$  point when  $\sigma$  drops to 0.2 eV, as shown in Fig. 1(b). The lowest acoustic phonon mode of monolayer  $\text{NbS}_2$  becomes lower and lower in energy at the  $M$  point as  $\sigma$  is reduced. When  $\sigma$  goes between 0.15 and 0.10 eV, the frequency of this soft mode becomes imaginary, which should give rise to a  $2 \times 2$  CDW phase in monolayer  $\text{NbS}_2$ , in good agreement with the previous results [30,47]. Although it was shown that the anharmonicity effect in  $\text{NbS}_2$

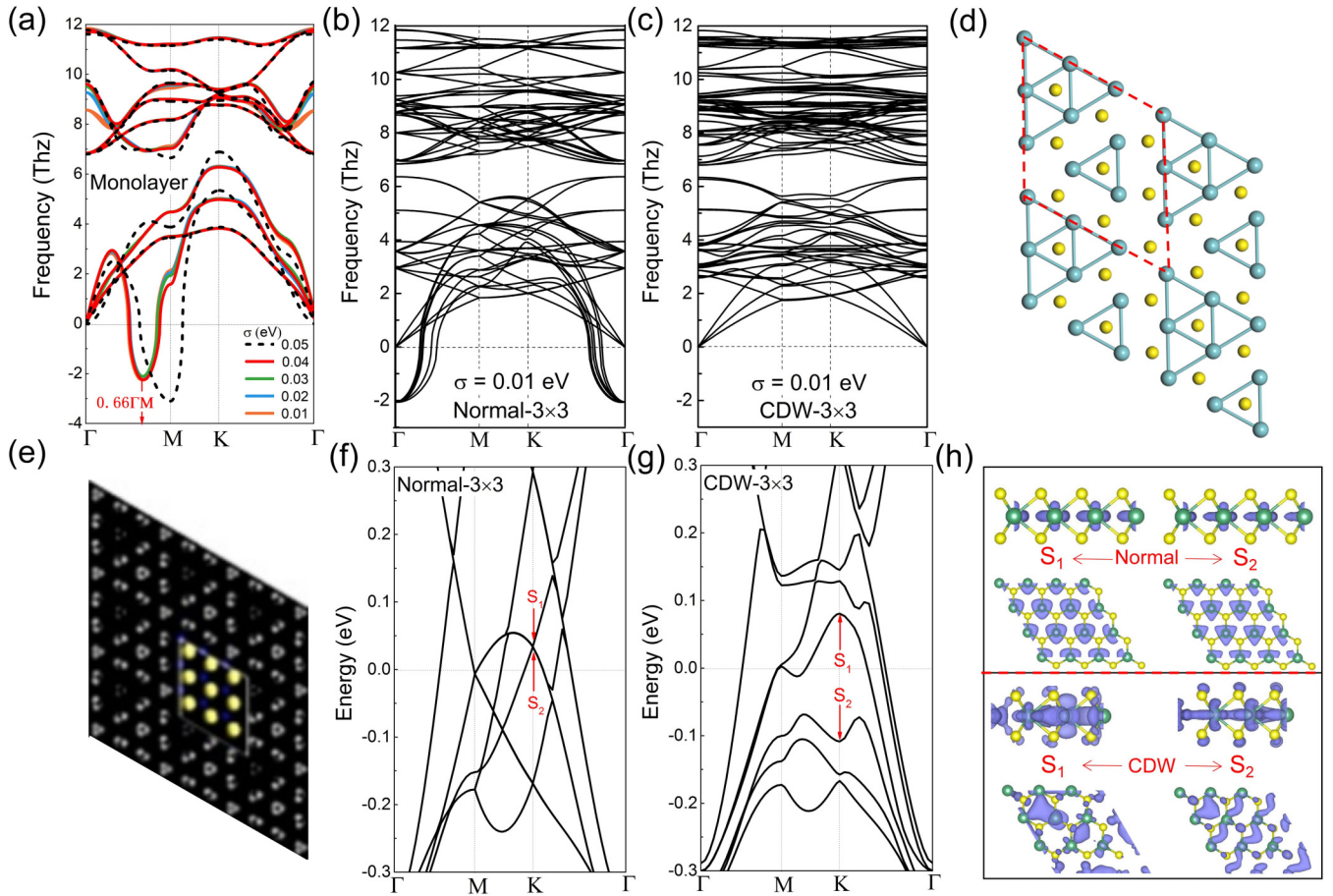


FIG. 2. The phonon dispersions of monolayer NbS<sub>2</sub> at different temperatures (a), the phonon dispersions of the 3 × 3 normal (b) and CDW (c) phases, the top view of the Nb sublattice in the 3 × 3 CDW phase (d) and the simulated STM image of the 3 × 3 CDW phase (e), the electronic bands near the Fermi level of the 3 × 3 normal (f) and CDW phases (g), and the charge densities of the states S<sub>1</sub> and S<sub>2</sub> at the K point near the Fermi level of the normal and CDW phases (h). The red dashed diamond in (d) indicates the 3 × 3 unit cell. The yellow dots in (e) indicate the S atom sites from the top view.

would hinder the realization of the 2 × 2 CDW phase, it is believed that NbS<sub>2</sub> is already very close to the limit of CDW phase transition.

We also calculated the phonon dispersions of bilayer [Fig. 1(c)] and trilayer [Fig. 1(d)] NbS<sub>2</sub>. It is found that at the temperature corresponding to  $\sigma = 0.1$  eV, the M point imaginary frequency of monolayer NbS<sub>2</sub> still persists in bilayer NbS<sub>2</sub>, but it becomes real and positive in trilayer NbS<sub>2</sub>. After  $\sigma$  is further reduced to 0.09 eV, the M point imaginary frequency emerges in trilayer NbS<sub>2</sub>.

It can be seen from Figs. 1(b), 1(c), and 1(d) that as the number of layers increases, the magnitude of the imaginary frequency is reduced, signifying that the CDW phase is more difficult to be realized within the harmonic model in thicker NbS<sub>2</sub> films.

### B. The CDW phases at lower temperatures

Recently, a 3 × 3 CDW modulation has been observed experimentally at very low temperature (4.6 K) when the thickness of NbS<sub>2</sub> on graphene/6H-SiC(0001) is reduced to one monolayer [33]. From the theoretical point of view, this 3 × 3 CDW modulation implies an instability in the phonon

spectrum at  $2/3 \Gamma M$ . To address the low-temperature 3 × 3 CDW phase in monolayer NbS<sub>2</sub>, we continue to reduce the  $\sigma$  to explore new possible instability. It is found that after the  $\sigma$  is decreased below 0.05 eV, the instability at the M-point disappears and simultaneously a new instability emerges at  $0.66 \Gamma M$  (very close to  $2/3 \Gamma M$ ) [Fig. 2(a)], which corresponds very well to the 3 × 3 structural modulation found in the experiments [33]. The anharmonic model also found an unstable mode at  $0.72 \Gamma M$ , which is near  $2/3 \Gamma M$  and should result in the 3 × 3 CDW phase [30]. It is further found that the unstable mode at  $2/3 \Gamma M$  is almost not changed if the anharmonicity is taken into account (see Fig. S1 in the Supplemental Material [48]), indicating that relaxation along this unstable mode would lead to basically the same 3 × 3 CDW phase for both harmonic and anharmonic models.

Until now, however, the atomic structure of this 3 × 3 CDW phase of monolayer NbS<sub>2</sub> was still undetermined, though it has been observed by scanning tunneling microscopy (STM) [33]. To reveal the 3 × 3 CDW structure, we first made an expansion of the 1 × 1 primitive cell of the monolayer NbS<sub>2</sub> to obtain an unrelaxed 3 × 3 structure, which will hereafter be referred to as the 3 × 3 normal phase or structure.  $\sigma$  is fixed at 0.01 eV. In the calculated phonon dispersion

of the  $3 \times 3$  normal phase, there are unstable modes at the  $\Gamma$  point [Fig. 2(b)], which correspond to the unstable modes at the  $2/3\Gamma$  point of the  $1 \times 1$  primitive cell [Fig. 2(a)] due to the Brillouin zone folding. The atoms in the  $3 \times 3$  normal structure are then displaced along the vibration direction of the unstable mode at the  $\Gamma$  point [Fig. 2(b)]. After atomic relaxation, a new  $3 \times 3$  CDW structure is stabilized with a total energy lowered by 11.6 meV, indicating that a phase transition takes place at very low temperatures. It is found that this  $3 \times 3$  CDW phase is dynamically stable since there is no imaginary frequency in the phonon bands [Fig. 2(c)]. In comparison with the  $3 \times 3$  normal phase with a uniform Nb-Nb distance of 3.3 Å, the relaxed  $3 \times 3$  structure is apparently less symmetric. The atomic relaxation results in the increase and decrease of the Nb-Nb distances. To better show the lattice distortion in the  $3 \times 3$  CDW structure, the Nb sublayer is displayed in Fig. 2(d) and Fig. S2 (see the Supplemental Material [48]), in which the distance between the connected Nb atoms is smaller than 3.26 Å whereas that between the unconnected neighboring Nb atoms is larger than 3.30 Å. The positions of S atoms remain almost the same as they are in the unrelaxed  $H$ -NbS<sub>2</sub>. We simulated the STM images of the  $3 \times 3$  CDW phase under the bias of 0.4 eV [Fig. 2(e)], in good agreement with the experiments [33].

Although the distortion in the  $3 \times 3$  CDW structure is small, the slight structural relaxation leads to appreciable changes of the electronic band structure with respect to that of the  $3 \times 3$  normal structure, as shown in Figs. 2(f) and 2(g). The symmetry breaking in  $3 \times 3$  CDW structure removes the degeneracies in the electronic bands of the normal  $3 \times 3$  structure and opens a gap around the  $K$  point near the Fermi level [Figs. 2(f) and 2(g)]. The charge distribution of the states [S1 and S2 states in Figs. 2(f) and 2(g)] at the  $K$  point near the Fermi level was calculated [Fig. 2(h)]. It can be found that in the normal phase, the charge is almost distributed on the Nb atoms and is quite symmetric. In the  $3 \times 3$  CDW phase, the charge is less concentrated on Nb atoms but becomes much more uneven and anisotropic, suggesting that the resistivity, sound velocity, etc., would be very different if measured in different directions.

In addition to the  $2/3\Gamma$  point in Fig. 2(a), instabilities may occur in different regions of the Brillouin zone. To explore whether there are other soft modes, we calculated the phonon dispersions over the whole first Brillouin zone with  $\sigma = 0.01$  eV and found all the imaginary frequencies, which are only populated near the  $2/3\Gamma$  point and its symmetric points (Fig. 3), suggesting that the monolayer NbS<sub>2</sub> may only have the  $3 \times 3$  CDW phase.

It was found that strains can modify the CDW phase [50]. We have made calculations about the effects of strain on the CDW phase in monolayer NbS<sub>2</sub>. Both the compressive and the tensile strains have been considered, as shown in Fig. 4. It can be seen that the  $3 \times 3$  CDW phase is fairly robust with respect to the small strains. Increasing the strains tends to weaken the  $3 \times 3$  CDW phase. Compressive strains larger than 4% and tensile ones larger than 5% will suppress the  $3 \times 3$  CDW phase.

The dissimilarities between the CDW behaviors of the similar NbS<sub>2</sub> and NbSe<sub>2</sub> have been a subject under discussion. The  $3 \times 3$  CDW phase is more difficult to be detected in

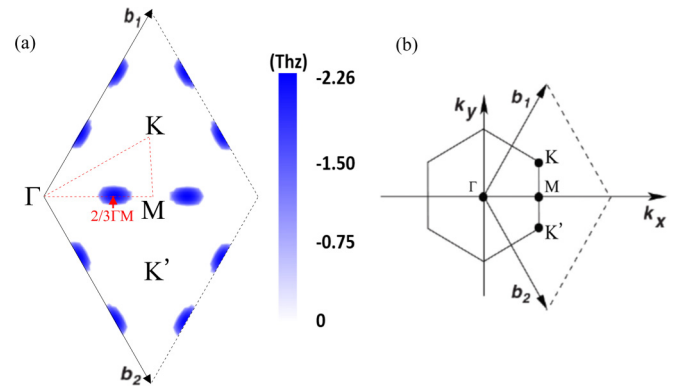


FIG. 3. (a) The distribution of the imaginary frequencies at low temperature [ $\sigma = 0.01$  eV, corresponding to Fig. 2(a)] in the first Brillouin zone. The imaginary frequencies are treated as negative real values. (b) The hexagonal Wigner-Seitz cell of the Brillouin zone with the high-symmetry points and the basis vectors  $\mathbf{b}_1$  and  $\mathbf{b}_2$  of the reciprocal space labeled.

NbS<sub>2</sub> than in NbSe<sub>2</sub>. It was found that the mass difference of S and Se atoms is not enough to explain these dissimilarities. We calculated the projected phonon densities of states (PPDOSs) of NbS<sub>2</sub> and NbSe<sub>2</sub> with  $\sigma = 0.01$  eV, as shown in Fig. 5. It is found that the Se atoms make a considerably larger contribution to the phonon density of states than the S atoms, suggesting that the former are much more active in vibration than the latter. To have a direct comparison, we also calculated the PPDOS of the Janus SeNbS, as shown in Fig. 5(b). The contribution of Se atoms is about twice as much as that of S atoms. Therefore, it is easier for the Se atoms to be displaced in the soft modes to enter the  $3 \times 3$  CDW phase, which might provide a perspective to understand why the  $3 \times 3$  CDW phase is easier to realize and observe in NbSe<sub>2</sub> than in NbS<sub>2</sub>.

We studied the tuning effect of electron doping on the CDW phase by adding a different number of electrons to monolayer NbS<sub>2</sub> and we calculated the phonon spectra. The  $\sigma$  parameter is fixed at 0.01 eV. At this low temperature, the

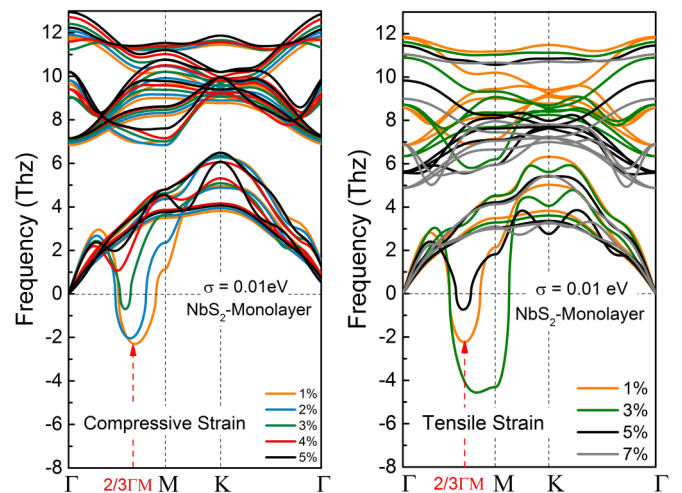


FIG. 4. The phonon dispersions of monolayer NbS<sub>2</sub> with  $\sigma = 0.01$  eV under different compressive (left) and tensile (right) strains.

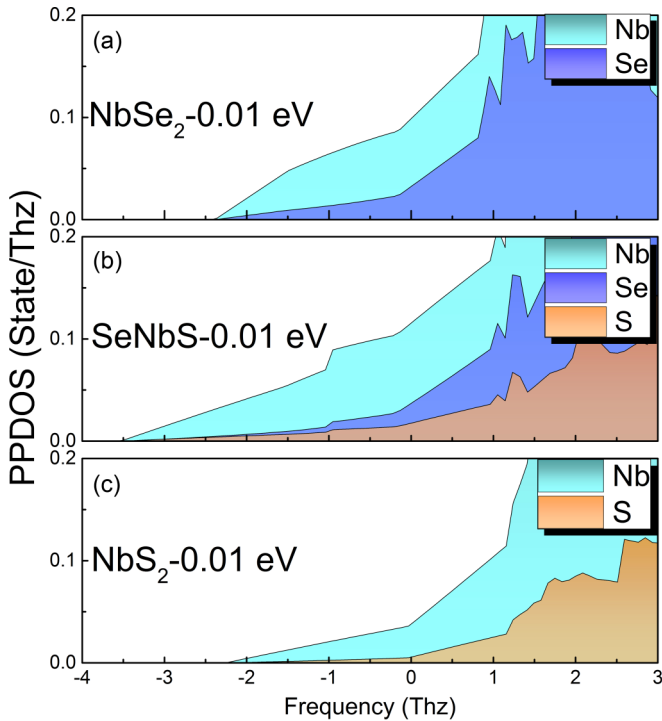


FIG. 5. The projected phonon densities of states of  $\text{NbS}_2$  (upper), Janus  $\text{SeNbS}$  (middle), and  $\text{NbS}_2$  (lower).

$3 \times 3$  CDW phase has been identified in the charge neutral case, as discussed above. In the following, the number of doped electrons refers to the number per formula unit. In Fig. 6, it can be found that at the very low doping level of  $0.005e$ , the instability at  $2/3\Gamma M$  is maintained. As the electron

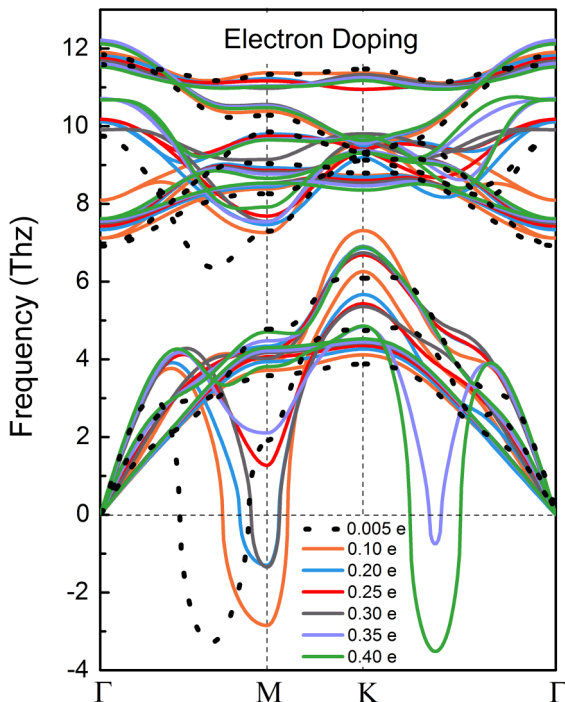


FIG. 6. Phonon dispersions of monolayer  $\text{NbS}_2$  under different electron doping levels.

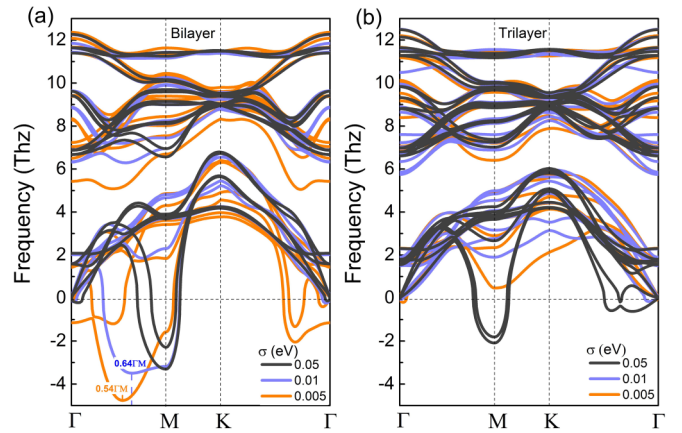


FIG. 7. The phonon dispersions at low temperatures for bilayer (a) and trilayer (b)  $\text{NbS}_2$ .

doping is increased from  $0.1e$  to  $0.2e$ , the unstable mode is moved to  $M$  point and hence the  $3 \times 3$  CDW phase will be removed. When the electron doping level reaches  $0.25e$ , the imaginary frequency is removed and no unstable mode is found. Continuing to dope electrons up to  $0.30e$ , an unstable mode reappears at the  $M$  point. Adding  $0.05e$  more electrons, it is observed that the  $M$  point unstable mode is suppressed and a new unstable mode emerges at  $1/4 K\Gamma$ , which suggests a  $4\sqrt{3} \times 4\sqrt{3}$  CDW phase [49].

The above rich phases induced by electron doping signify that the sample preparation and measurements which may introduce charge doping will affect the observation of the CDW phases in experiments. The CDW phase was not observed in  $\text{NbS}_2$  grown on the  $\text{Au}(111)$  surface and hence the existence of  $\text{NbS}_2$  CDW phase was questioned [32]. However, a  $3 \times 3$  CDW phase was identified in  $\text{NbS}_2$  grown on graphene/ $\text{SiC}(0001)$  [33]. The appearance of the  $3 \times 3$  CDW phase is therefore substrate-dependent. One important difference between these two substrates is that  $\text{Au}(111)$  as a metal is a better electron dopant than graphene, which is a semimetal. We calculated the  $\text{NbS}_2/\text{Au}(111)$  and  $\text{NbS}_2/\text{graphene}$  systems and performed Bader charge analysis to study the electron transfer from the substrate to  $\text{NbS}_2$ . It is found that  $\text{NbS}_2$  per formula unit obtains  $0.176e$  from  $\text{Au}(111)$ , which is sufficient to suppress the  $3 \times 3$  CDW phase according to the electron doping induced CDW phases discussed above (see Fig. 6). The electron doping level from monolayer and bilayer graphene to  $\text{NbS}_2$  significantly reduces to only  $0.044e$  and  $0.0046e$ , respectively, which is low enough to keep the  $3 \times 3$  CDW phase (see Fig. 6). Although the substrate effects are complex and usually cannot be ascribed to one single factor, the difference of the electron doping contributed by  $\text{Au}(111)$  and graphene is already large enough to affect the CDW phase in  $\text{NbS}_2$ , leading to different experimental observations [32].

We also searched the possible low-temperature CDW phases of the bilayer and trilayer  $\text{NbS}_2$ . For bilayer  $\text{NbS}_2$  [Fig. 7(a)], it is found that there is also imaginary frequencies at the  $M$  point with  $\sigma = 0.05$  eV, indicating that the  $2 \times 2$  CDW phase may exist in bilayer  $\text{NbS}_2$ . The instability is shifted from the  $M$  point to  $0.64\Gamma M$  ( $\sim 2/3\Gamma M$ ) when the temperature is reduced to  $\sigma = 0.01$  eV [Fig. 7(a)], indicating

that bilayer NbS<sub>2</sub> can also have the  $3 \times 3$  CDW phase. After the temperature is further lowered down to  $\sigma = 0.005$  eV, the unstable mode is found to be shifted to  $0.54 \Gamma M$  ( $\sim 1/2 \Gamma M$ ), as shown in Fig. 7(a), suggesting that a new  $4 \times 4$  CDW phase could appear in the very low temperature region. For trilayer NbS<sub>2</sub>, it is found that the M point unstable mode in the high-temperature region [Fig. 7(b)] extends to the low-temperature region corresponding to  $\sigma = 0.05$  eV, as opposed to the cases of monolayer and bilayer, in which the unstable mode is shifted from M to  $2/3 \Gamma M$  point. When the temperature is further reduced ( $\sigma < 0.01$  eV), it is found that the unstable mode at the M point vanishes. Therefore, the  $3 \times 3$  CDW phase that could appear in monolayer and bilayer NbS<sub>2</sub> may not be shown in trilayer NbS<sub>2</sub>. The layer-dependent CDW phases indicate that the interlayer interaction can effectively tune the CDW phases of the layered systems.

#### IV. CONCLUSIONS

In summary, we have explored the CDW phases of monolayer, bilayer, and trilayer NbS<sub>2</sub>. It is found that there is a soft mode at the M point at higher temperature ( $0.05 < \sigma < 0.2$  eV) for monolayer NbS<sub>2</sub>. At lower temperature ( $\sigma < 0.05$  eV), an unstable mode develops at the point very close to  $2/3 \Gamma M$ , which corresponds to the experimentally observed  $3 \times 3$  CDW phase. It is shown that this unstable mode is almost unchanged if anharmonicity is considered. We searched the possible unstable modes throughout the Brillouin zone and found that the instabilities only occur around the  $2/3 \Gamma M$  point and its symmetrically equivalent points. By atomic displacements along the unstable vibrational modes, the instability is removed and a stable  $3 \times 3$  CDW structure with lower total energy is determined. We simulated STM images of the  $3 \times 3$  CDW structure, which agree well with the experimental observation. With the breaking of the symmetries, many degeneracies in the electronic bands of the normal phase are lifted after the formation of  $3 \times 3$  CDW phase, opening a band

gap around the K point. At the same time, the charge distribution becomes highly asymmetric, which can induce large anisotropy in electronic, thermal, and mechanical properties. We made a comparison of the PDOSs of NbS<sub>2</sub>, NbSe<sub>2</sub>, and Janus SeNbS, revealing that the Se atoms are much more vibrationally dynamic than the S atoms, which provides a new perspective to understand why the CDW phase in NbSe<sub>2</sub> is easier to observe. Doping electrons to monolayer NbS<sub>2</sub> can bring about a sequence of CDW phase transitions from  $3 \times 3$  to  $2 \times 2$  and to  $4\sqrt{3} \times 4\sqrt{3}$  structures when the doping level is increased from  $0.1e$  to  $0.4e$ . It is found that there are significantly more electrons transferred from Au(111) to NbS<sub>2</sub> than from graphene, which provides a key to understanding why the  $3 \times 3$  CDW phase is observed in NbS<sub>2</sub>/graphene but not in NbS<sub>2</sub>/Au(111). The phonon dispersions of monolayer NbS<sub>2</sub> were calculated under different compressive and tensile strains. It is found that the  $3 \times 3$  CDW phase is maintained under small strains, seeming to suggest that the induced strains in substrate supported NbS<sub>2</sub> may not be as relevant as charge doping in tuning the CDW phase within the harmonic model. The interlayer interaction has considerable influence on the CDW phase transitions in bilayer and trilayer NbS<sub>2</sub>. In bilayer NbS<sub>2</sub>, a series of instabilities occur corresponding to  $2 \times 2$ ,  $3 \times 3$ , and  $4 \times 4$  CDW phases with the dropping of the temperature. For trilayer NbS<sub>2</sub>, on the other hand, only a  $2 \times 2$  CDW phase is found. The  $3 \times 3$  CDW phase that exists in monolayer and bilayer NbS<sub>2</sub> is not found in trilayer NbS<sub>2</sub>. In the lower temperature end, the trilayer NbS<sub>2</sub> tends to be stable instead.

#### ACKNOWLEDGMENTS

The authors acknowledge the support of the National Natural Science Foundation of China (Grants No. 11874315 and No. 11874316), the National Basic Research Program of China (2015CB921103), the Innovative Research Team in University (No. IRT 17R91), and Hunan Provincial Innovation Foundation for Postgraduate (Grant No. CX20190472).

- 
- [1] A. H. Castro Neto, *Phys. Rev. Lett.* **86**, 4382 (2001).
  - [2] K. Rossnagel, *J. Phys. Condens. Matter* **23**, 213001 (2011).
  - [3] M. Calandra, I. I. Mazin, and F. Mauri, *Phys. Rev. B* **80**, 241108(R) (2009).
  - [4] G. Wexler and A. Woolley, *J. Phys. C* **9**, 1185 (1976).
  - [5] P. Ganguly and A. K. Jha, *Physica B* **405**, 3154 (2010).
  - [6] J. van Wezel, *Europhys. Lett.* **96**, 67011 (2011).
  - [7] T. Ritschel, J. Trinckauf, K. Koepf, B. Büchner, M. v. Zimmermann, H. Berger, Y. Joe, P. Abbamonte, and J. Geck, *Nat. Phys.* **11**, 328 (2015).
  - [8] Z. Y. Zhu, Y. C. Cheng, and U. Schwingenschlögl, *Phys. Rev. B* **84**, 153402 (2011).
  - [9] H.-P. Komsa and A. V. Krasheninnikov, *Phys. Rev. B* **88**, 085318 (2013).
  - [10] C.-H. Chang, X. Fan, S.-H. Lin, and J.-L. Kuo, *Phys. Rev. B* **88**, 195420 (2013).
  - [11] C. Luo, X. Peng, J. Qu, and J. Zhong, *Phys. Rev. B* **101**, 245416 (2020).
  - [12] M. D. Johannes and I. I. Mazin, *Phys. Rev. B* **77**, 165135 (2008).
  - [13] J. Wilson, F. Di Salvo, and S. Mahajan, *Phys. Rev. Lett.* **32**, 882 (1974).
  - [14] J. A. Wilson, F. Di Salvo, and S. Mahajan, *Adv. Phys.* **24**, 117 (1975).
  - [15] M. M. Ugeda *et al.*, *Nat. Phys.* **12**, 92 (2016).
  - [16] K. Rossnagel, O. Seifarth, L. Kipp, M. Skibowski, D. Voß, P. Krüger, A. Mazur, and J. Pollmann, *Phys. Rev. B* **64**, 235119 (2001).
  - [17] F. Weber, S. Rosenkranz, J. P. Castellán, R. Osborn, R. Hott, R. Heid, K. P. Bohnen, T. Egami, A. H. Said, and D. Reznik, *Phys. Rev. Lett.* **107**, 107403 (2011).
  - [18] A. Soumyanarayanan, M. M. Yee, Y. He, J. Van Wezel, D. J. Rahn, K. Rossnagel, E. W. Hudson, M. R. Norman, and J. E. Hoffman, *Proc. Natl. Acad. Sci. (USA)* **110**, 1623 (2013).
  - [19] C.-S. Lian, C. Si, J. Wu, and W. Duan, *Phys. Rev. B* **96**, 235426 (2017).
  - [20] D. Pasquier and O. V. Yazyev, *Phys. Rev. B* **98**, 045114 (2018).

- [21] X.-L. Yu, D.-Y. Liu, Y.-M. Quan, J. Wu, H.-Q. Lin, K. Chang, and L.-J. Zou, *Phys. Rev. B* **96**, 125138 (2017).
- [22] Y. Chen *et al.*, *Adv. Mater.* **32**, 2003746 (2020).
- [23] P. Anderson, P. Lee, and M. Saitoh, *Solid State Commun.* **13**, 595 (1973).
- [24] R. E. Peierls, *Quantum Theory of Solids* (Clarendon Press, Oxford, 1996).
- [25] M. Calandra, *Nat. Nanotechnol.* **10**, 737 (2015).
- [26] X. Xi, L. Zhao, Z. Wang, H. Berger, L. Forró, J. Shan, and K. F. Mak, *Nat. Nanotechnol.* **10**, 765 (2015).
- [27] M. Leroux, L. Cario, A. Bosak, and P. Rodiere, *Phys. Rev. B* **97**, 195140 (2018).
- [28] I. Guillamón, H. Suderow, S. Vieira, L. Cario, P. Diener, and P. Rodiere, *Phys. Rev. Lett.* **101**, 166407 (2008).
- [29] A. Y. Liu, *Phys. Rev. B* **79**, 220515(R) (2009).
- [30] R. Bianco, I. Errea, L. Monacelli, M. Calandra, and F. Mauri, *Nano Lett.* **19**, 3098 (2019).
- [31] C. Wen, Y. Xie, Y. Wu, S. Shen, P. Kong, H. Lian, J. Li, H. Xing, and S. Yan, *Phys. Rev. B* **101**, 241404(R) (2020).
- [32] R.-M. Stan, S. K. Mahatha, M. Bianchi, C. E. Sanders, D. Curcio, P. Hofmann, and J. A. Miwa, *Phys. Rev. Materials* **3**, 044003 (2019).
- [33] H. Lin, W. Huang, K. Zhao, C. Lian, W. Duan, X. Chen, and S.-H. Ji, *Nano Res.* **11**, 4722 (2018).
- [34] G. Kresse and J. Furthmüller, *Comput. Mater. Sci.* **6**, 15 (1996).
- [35] G. Kresse and J. Furthmüller, *Phys. Rev. B* **54**, 11169 (1996).
- [36] J. Hafner, *J. Comput. Chem.* **29**, 2044 (2008).
- [37] P. E. Blöchl, *Phys. Rev. B* **50**, 17953 (1994).
- [38] M. Calandra and F. Mauri, *Phys. Rev. Lett.* **95**, 237002 (2005).
- [39] F. Weber, S. Rosenkranz, J.-P. Castellán, R. Osborn, G. Karapetrov, R. Hott, R. Heid, K.-P. Bohnen, and A. Alatas, *Phys. Rev. Lett.* **107**, 266401 (2011).
- [40] M. Verstraete and X. Gonze, *Phys. Rev. B* **65**, 035111 (2001).
- [41] F. Weber, R. Hott, R. Heid, K. P. Bohnen, S. Rosenkranz, J. P. Castellán, R. Osborn, A. H. Said, B. M. Leu, and D. Reznik, *Phys. Rev. B* **87**, 245111 (2013).
- [42] D. L. Duong, M. Burghard, and J. C. Schön, *Phys. Rev. B* **92**, 245131 (2015).
- [43] C. Chen, B. Singh, H. Lin, and V. M. Pereira, *Phys. Rev. Lett.* **121**, 226602 (2018).
- [44] F. Weber, L. Pintschovius, W. Reichardt, R. Heid, K. P. Bohnen, A. Kreyssig, D. Reznik, and K. Hradil, *Phys. Rev. B* **89**, 104503 (2014).
- [45] A. Togo and I. Tanaka, *Scr. Mater.* **108**, 1 (2015).
- [46] F. Güller, V. L. Vildosola, and A. M. Llois, *Phys. Rev. B* **93**, 094434 (2016).
- [47] M. Leroux, M. Le Tacon, M. Calandra, L. Cario, M. A. Measson, P. Diener, E. Borrisenko, A. Bosak, and P. Rodiere, *Phys. Rev. B* **86**, 155125 (2012).
- [48] See Supplemental Material at <http://link.aps.org/supplemental/10.1103/PhysRevB.105.174105> for the anharmonic unstable vibrational mode at the  $2/3 \Gamma M$  point and the detailed description of the atomic structure of the Nb sublayer in the  $3 \times 3$  CDW phase.
- [49] E. Kamil, J. Berges, G. Schonhoff, M. Rosner, M. Schuler, G. Sangiovanni, and T. O. Wehling, *J. Phys. Condens. Matter* **30**, 325601 (2018).